

the reststrahlen frequency region with decreasing particle size. Not only is detail lost in the minimum, but also there is an increase in the departure of the minimum from unity. This result is in agreement with that of Goetz (3). For the two samples of small particle size (0 to 74  $\mu$  and 0 to 5  $\mu$ ), where scattering is important, a well-defined maximum appears and its spectral contrast increases with decreasing particle size.

Figure 2A shows the effective emissivity spectra of a hornblende sample recorded under three different experimental conditions which alter the energy distribution within the sample. The spectral contrast of the emissivity maximum is increased as the pressure is decreased or as the temperature of the radiation shield is lowered.

In these samples thermal conductivity at high (atmospheric) pressure is dominated by heat conduction through whatever gas separates the particles, but this form of heat transfer is precluded in our low-pressure experiments, where evacuation lowers the conductivity by an order of magnitude (4). In this latter case the dominant mechanism becomes radiative transfer. Then radiation to a cold background is so efficient in cooling the surface layers that a sharp thermal gradient can be established very near the surface, despite the fact that the sample is heated through this surface by visible radiation from the lamp (sun). This will be true whenever the average optical depth is greater over the wavelength range of radiative heating (visible to near-infrared) than it is for radiative cooling at longer wavelengths.

The magnitude of the temperature gradient is determined by (i) the heating profile; (ii) the radiative cooling efficiency, which is related to the probability of photon escape through the surface as a function of depth at all wavelengths; and (iii) the difference in temperature between the bulk sample and the background to which the sample radiates. The greater this temperature difference, the sharper is the gradient established in any sample for a given pressure.

For a well-defined maximum to appear in an emission spectrum, the thermal gradient must occur on the same depth scale as the optical depths of the photons in the envelope of the maximum. In such a case, variations in optical depth with wavelength (demonstrated by the transmission spectrum) will map the extent to which energy

can escape from the deeper, hotter regions of the sample. The correlation between the transmission and emissivity spectra shown in Fig. 2 is consistent with this explanation, as is the change in spectral contrast of the three emissivity spectra. As can be seen, the spectral contrast is greatest for those experimental conditions which produce the sharpest thermal gradient at the surface of the sample.

This explanation is highly oversimplified but a more rigorous treatment involving radiative transfer mechanisms and consideration of exactly how the photon concentration profiles are generated leads to the same general conclusion. The important point here is that, the more closely the lunar thermal conditions are simulated, the greater is the spectral contrast of the emissivity maximum.

Figure 3 shows the emissivity spectra recorded under the same experimental conditions of several materials having the same grain size but different composition. It is apparent that the position of the emissivity maximum is as diagnostic of composition as the reststrahlen features in reflection spectra. Moreover, the departure of the emissivity minimum from unity is widely variable, with the general trend being that the more acidic materials with higher albedos display greater departures than

the more basic samples with lower albedos. Artificial alteration of the albedo of the gabbro sample by the addition of up to 50 percent ilmenite gives rise to a loss of contrast, but the characteristic emissivity maximum is not shifted.

From these preliminary results we conclude that both the thermal environment and the surface texture make the moon, and probably Mercury, unusually suitable targets for compositional remote sensing by mid-infrared spectroscopic techniques. A fuller report of the work discussed here will be presented elsewhere (5). It appears that the technique can be used to define general rock type.

LLOYD M. LOGAN, GRAHAM R. HUNT  
*Spectroscopic Studies Branch,  
Air Force Cambridge Research  
Laboratories, L. G. Hanscom Field,  
Bedford, Massachusetts 01730*

#### References

1. R. A. Van Tassel and I. Simon, in *The Lunar Surface Layer*, J. Salisbury and P. Glazer, Eds. (Academic Press, New York, 1964), pp. 445-468; R. J. P. Lyon, "Final Report, Part II, NASA Contract No. NaSr-49(04)" (1964).
2. J. E. Conel, *J. Geophys. Res.* **74**, 1614 (1969).
3. A. F. H. Goetz, thesis, California Institute of Technology (1967).
4. J. W. Salisbury and P. E. Glazer, *Air Force Cambridge Res. Lab. 60-70 Spec. Rep. No. 20* (1964).
5. L. M. Logan and G. R. Hunt, *J. Geophys. Res.*, in press.

21 April 1970; revised 26 June 1970

## Orthopyroxene-Plagioclase Fragments in the Lunar Soil from Apollo 12

**Abstract.** *Rock fragments consisting of orthopyroxene-calcic plagioclase assemblages appear to be more common in Apollo 12 soil samples than in the breccias or soil from Apollo 11 and are mineralogically and chemically different from any of the crystalline rocks returned by either Apollo 11 or Apollo 12. Compositionally, these fragments are orthopyroxenites and feldspathic orthopyroxenites. They are probably not fragments of meteorites; other considerations point to a near-surface lunar origin.*

Several lithic fragments consisting of orthopyroxene, (Mg,Fe)SiO<sub>3</sub>, and calcic plagioclase have been identified in a small amount (30 mg) of the Apollo 12 lunar soil, sample No. 12070,61. No equivalent rock type has been found in any of the Apollo 11 crystalline rocks nor apparently in any of the Apollo 12 rocks, as judged from preliminary reports of the Lunar Sample Preliminary Examination Team (1).

Clinopyroxene, (Ca,Mg,Fe)SiO<sub>3</sub>, is a major constituent in the Apollo 11 soil and in all of the Apollo 11 rocks. It appears that orthopyroxene, with only

minor Ca, occurs in trace amounts in the soil and breccia samples, since it was reported by relatively few investigators. Albee *et al.* (2) found a fragment in the soil, which they designated Luny Rock 1, to consist of orthopyroxene, isotropic plagioclase, "K-feldspar," ilmenite, troilite, apatite, whitlockite, and a rare-earth calcium phosphate mineral. Douglas *et al.* (3) reported plagioclase-orthopyroxene fragments in several breccias; Keil *et al.* (4) found the assemblage maskelynite, clinopyroxene, and orthopyroxene in a breccia; and Arrhenius *et al.* (5) reported that

one soil fragment contained a high proportion of calcic plagioclase coexisting with olivine and orthopyroxene. Although the chemical and mineralogical dissimilarities between these mineral assemblages and the crystalline rocks were recognized, it was not generally apparent that these rare occurrences might represent distinct rock types on the lunar surface. Albee *et al.* suggested that Luny Rock 1, one of the oldest dated of the Apollo 11 rock fragments, did not represent a mare sample.

It may be fortuitous, but it appears that orthopyroxene-plagioclase associations may be more prevalent in the Apollo 12 soil. Three such fragments were identified in a 30-mg sample. In addition to these, two orthopyroxene grains were found. The three fragments measure from 1 to 1.5 mm in diameter and contain fine-grained anhedral crystals of predominantly orthopyroxene with lesser amounts of untwinned plagioclase and trace amounts of accessory minerals. The largest grains of the two major minerals are 100  $\mu\text{m}$  across but most average 50  $\mu\text{m}$ , the accessory minerals are 25  $\mu\text{m}$  and smaller. The small grain size argues against crystallization in a deep-seated environment; the possibility of near-surface recrystallization of material formed at depths will be discussed later.

Identification of orthopyroxene in all five of the presently reported occurrences was confirmed by x-ray powder patterns, since compositions alone are not sufficient to distinguish low Ca clinopyroxene from orthopyroxene. The patterns indicate an ordered structure based on the criteria noted by Pollack and Ruble (6).

Compositions of the orthopyroxenes in the three rock fragments A, B, and C are given in Table 1. Expressed in terms of the end-member molecules Wo ( $\text{CaSiO}_3$ ), En ( $\text{MgSiO}_3$ ), and Fs ( $\text{FeSiO}_3$ ), representative formulas are: (A)  $\text{Wo}_4\text{En}_{59}\text{Fs}_{35}$ , (B)  $\text{Wo}_2\text{En}_{82}\text{Fs}_{16}$ , and (C)  $\text{Wo}_4\text{En}_{65}\text{Fs}_{31}$ . Some of the orthopyroxene grains in A contain irregular narrow lamellae of the clinopyroxene augite, approximate composition  $\text{Wo}_{38}\text{En}_{39}\text{Fs}_{23}$ , exsolved parallel to the optic axial plane of the host. The mineral composition of the fragments are (in percent by volume): (A) orthopyroxene, 60; plagioclase ( $\text{An}_{82}$ ), 35; ilmenite, 4; troilite, 1; and less than 1 of metallic Fe, a phosphate mineral, and a K-rich aluminum silicate; (B) orthopyroxene, 70; and plagioclase ( $\text{An}_{90}$ ), 30; and (C) orthopyroxene, 87; plagioclase ( $\text{An}_{75}$ ), 10; ilmenite, 2;

Table 1. Electron microprobe analyses (percent by weight) of orthopyroxene from three rock fragments (A, B, and C) in Apollo 12 soil sample 12070,61.  $\text{K}_2\text{O}$  and  $\text{Na}_2\text{O}$  were below background. Standard used was hypersthene from the Johnstown achondritic meteorite (9). No corrections, other than background, were applied.

	A (average of eight grains)	B (average of six grains)	C (average of three grains)
$\text{SiO}_2$	54.4	56.4	54.8
$\text{Al}_2\text{O}_3$	0.3	0.3	0.2
$\text{Cr}_2\text{O}_3$	0.4	0.5	0.3
$\text{TiO}_2$	1.1	0.7	1.0
FeO	21.3	10.6	19.0
MgO	21.3	31.7	23.9
CaO	2.0	1.2	1.8
MnO	0.3	0.2	0.3

and augite, 1. The composition of the only phosphate grain (15  $\mu\text{m}$ ) in A is unique because of its high rare-earth content (in percent by weight):  $\text{P}_2\text{O}_5$ , 42.3; CaO, 42.5; FeO, 1.3; MgO, 3.2;  $\text{Na}_2\text{O}$ , 0.5;  $\text{La}_2\text{O}_3$ , 1.0;  $\text{Ce}_2\text{O}_3$ , 2.8;  $\text{Pr}_2\text{O}_3$ , 0.3;  $\text{Nd}_2\text{O}_3$ , 0.8;  $\text{Gd}_2\text{O}_3$ , 0.5;  $\text{Dy}_2\text{O}_3$ , 0.4;  $\text{Ho}_2\text{O}_3$ , 0.4; and  $\text{Y}_2\text{O}_3$ , 2.8; no europium above 0.1 was detected. Small amounts of  $\text{Er}_2\text{O}_3$ ,  $\text{Sm}_2\text{O}_3$ , and  $\text{Lu}_2\text{O}_3$  are present; respective estimates (factor of 2) are 0.2, 0.3, and 0.1 but no standards were available. In practically all respects, A is qualitatively similar to Luny Rock 1 found in the Apollo 11 soil by Albee *et al.* (2).

The mineral compositions suggest that A and B are feldspathic orthopyroxenites and that C is essentially equivalent to an orthopyroxenite. Such rock types occur terrestrially in stratified igneous complexes as differentiates developed by fractional crystallization of basaltic magmas. Similarly, the lunar occurrences could have formed as differentiates from the source magma of the Apollo 11 crystalline rocks. On the basis of experimental studies, Ringwood and Essene (7) suggested that the Apollo 11 basalt originated at depths of 200 to 400 km by a small degree of partial melting of pyroxenitic source material in which orthopyroxene predominates over clinopyroxene. This model, then, indicates a likely source of orthopyroxene in the lunar interior.

A possibility, albeit small, exists that these fragments are meteoritic in origin. Possible candidates are the hypersthene and the pyroxene-plagioclase achondrites. The latter include the howardites and eucrites, but the eucrites may be excluded as they contain more of the clinopyroxene (pigeonite) than the orthopyroxene (hypersthene), whereas hypersthene exceeds the amount of pi-

geonite in the howardites according to Mason (8). Mason gives the range in the  $\text{FeO}/(\text{FeO} + \text{MgO})$  ratio (mole percent) for hypersthene in the howardites as 25 to 40. The orthopyroxene from fragment A, 37 percent, and from C, 32 percent, fall within this range. That from B, 16 percent, is too low to be included in the howardites or the hypersthene achondrites for which the range is from 20 to 30 percent (8). The relatively high  $\text{TiO}_2$  contents of these lunar orthopyroxenes suggest a non-meteoritic origin, but little information exists on  $\text{TiO}_2$  contents of orthopyroxenes from achondrites for comparison. Orthopyroxene in the hypersthene achondrites Johnstown and Tatahouine contains 0.2 (by weight) percent of  $\text{TiO}_2$  (9), which is less than 30 percent of the lowest value quoted in Table 1. A meteoritic origin for fragment B is thus excluded on two counts. A similar exclusion for A and C is based on their calculated contents of bulk  $\text{TiO}_2$ , 3.9 and 2.5 percent by weight, which greatly exceed the  $\text{TiO}_2$  contents for the howardites Bununu (0.1) and Frankfort (0.5) (8), and Kapoeta, (0.4) (10).

The fragments then, if not meteoritic, must be indigenous to the moon, but whether they represent deep-seated or near-surface rocks, cannot be resolved easily. It was previously pointed out in this report that the small grain size argues against a deep-seated origin. If the parent rocks were pyroxenite, then some process must have occurred which raised them to a near-surface site where they were quenched from either a molten or semifluid state. Even neglecting the small grain size, a problem exists of mobilizing a high-temperature melt of pyroxenitic composition to the lunar surface without its dissolving basalt in transit. Alternatively, the fragments may be local accumulations in a parent rock whose bulk composition was not that of a pyroxenite. In any event, if the mineral composition of these three orthopyroxene-plagioclase fragments are representative of larger rocks, then a lunar occurrence of rock types distinct from any of those returned by either Apollo 11 or Apollo 12 is indicated.

LOUIS H. FUCHS

Argonne National Laboratory,  
Argonne, Illinois 60439

#### References and Notes

1. Lunar Sample Preliminary Examination Team, *Science* 167, 1325 (1970).
2. A. L. Albee, D. S. Burnett, A. A. Chodos, O. J. Eugster, J. C. Huneke, D. A. Papanastasiou, F. A. Podeseck, G. Price Russ II, H.

- G. Sanz, F. Tera, G. J. Wasserburg, *ibid.*, p. 463.
3. J. A. V. Douglas, M. R. Dence, A. G. Plant, R. J. Traill, *ibid.*, p. 594.
4. K. Keil, M. Prinz, and T. E. Bunch, *ibid.*, p. 597.
5. G. Arrhenius, S. Asunmaa, J. I. Drever, J. Everson, R. W. Fitzgerald, J. Z. Frazer, H. Fujita, J. S. Hanor, D. Lal, S. S. Liang, D. MacDougall, A. M. Reid, J. Sinkankas, L. Wilkening, *ibid.*, p. 659.
6. S. S. Pollack and W. D. Ruble, *Amer. Mineral.* 49, 983 (1964).
7. A. E. Ringwood and E. Essene, *Science* 167, 607 (1970).
8. B. Mason, *Geochim. Cosmochim. Acta* 31, 107 (1967).
9. ———, *Amer. Mus. Novitates*, No. 2155 (1963).
10. ——— and H. B. Wiik, *ibid.*, No. 2273 (1966).
11. Based on work performed under the auspices of AEC and by NASA contract T-76536. I thank J. Sanecki for microprobe results, and G. Montet for a review of the manuscript, both of Argonne National Laboratory. Helpful discussions were held with E. Olsen of the Field Museum of Natural History and Brian Mason of the U.S. National Museum.

19 June 1970

## Sintered Diamond: A Synthetic Carbonado

**Abstract.** *Diamond powder is rapidly sintered into molded shapes at a pressure of about 65 kilobars and a temperature of 2500° Kelvin. Other conditions of pressure and temperature are also suitable. The product compares favorably with natural carbonado in its properties.*

A dozen years ago, I discussed the desirability and possibility of preparing a carbonado-type substance by bonding diamond particles together under conditions of high pressure and high temperature (1). I now report procedures for accomplishing this.

Natural carbonado is a rare polycrystalline form of diamond found primarily in Brazil. Because of its toughness it is sometimes used in diamond drilling bits for penetrating hard rock formations. Carbonado would have many additional uses if it were more readily available and if it were less difficult to shape. It has no regular cleavage, as does ordinary diamond, and it is also much more difficult to cut and polish. These problems are overcome in the synthetic carbonado, because it can be formed to shape in a mold. Several sintered diamond articles, including a cylinder with an axial

hole strung on a wire are shown in Fig. 1.

The synthetic material is tough. It cuts, indents, scratches, abrades, and wears well. Compressive strengths ranging up to 58 kb and densities up to 3.48 g/cm<sup>3</sup> (the theoretical density of single crystal diamond is 3.51) have been measured.

I have experimentally delineated practical pressure and temperature fields, wherein pure diamond powder can be sintered within times ranging from several days down to about a second. This is illustrated by Fig. 2, where line 1 separates the thermodynamic region of stability for diamond (above line 1) from that of graphite (below line 1). Line 3 indicates a somewhat arbitrary lower temperature limit for obtaining a usable sintered body. Sintering times at this temperature are several days.

Line 2 delineates a practical region of stability where diamond powder is kinetically stable (metastable) with respect to conversion to graphite. This region is located between lines 1 and 2. The thermodynamic equilibrium (line 1) is, of course, time-independent. However, metastability (line 2) depends on time. The line shown is that determined for a temperature holding time of 30 minutes. For other heating times, the shape of the line is similar, but its position is shifted. The diamond powder is first subjected to pressure. Temperature is then applied and held constant for 30 minutes, after which the sample is quenched to room temperature before pressure is released. A longer temperature holding time reduces the area between lines 1 and 2, whereas a shorter time increases the area. Line 2 is also affected somewhat by diamond particle size, impurities, surface characteristics, and the surrounding atmosphere. A distinctive feature of line 2 is the large change in slope occurring near a pressure of 35 kb and a temperature of 1400°K.

Diamond powder can be sintered into a coherent body without any transformation into nondiamond forms of carbon in the region between lines 2 and 3. It is important to note that although this region includes and overlaps the region of diamond thermodynamic stability, it is not necessary to work within the region of thermodynamic stability to produce sintered diamond.

At a given pressure, sintering is most rapid at a temperature near line 2. Sintering time decreases rapidly with increasing temperature; consequently, the shortest sintering time is achieved at the highest pressure. It is possible to obtain a well-sintered product in only a few seconds at 85 kb.

For the particular heating time for which line 2 has been determined and a given pressure, line 2 determines the highest temperature than can be used to produce sintered diamond without any transformation to nondiamond carbon. Sintered diamond made under these circumstances is white or translucent in color.

Contrary to my former expectations, a sintered diamond product can be made at temperatures higher than those designated by line 2. At these temperatures some of the diamond will transform to nondiamond carbon. This product is black in color.

Therefore, careful regulation of temperature about those designated by

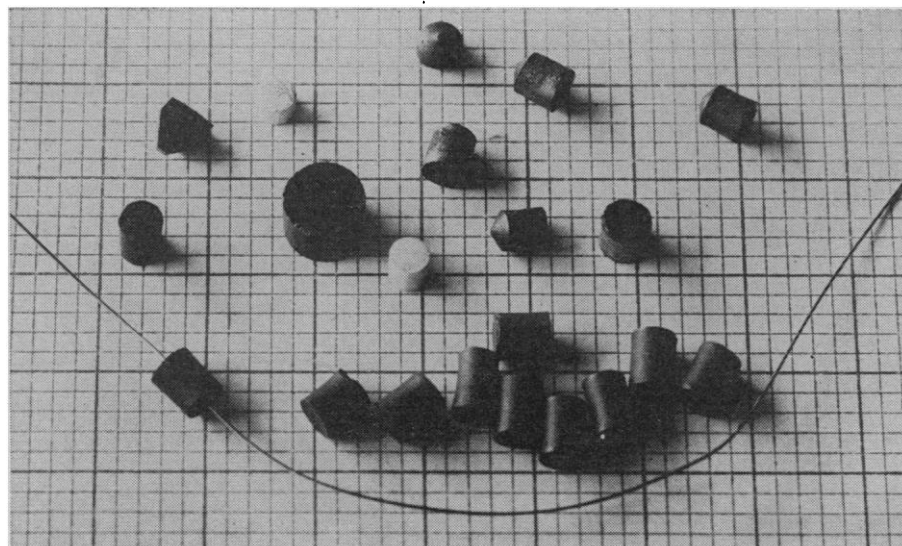


Fig. 1. Sintered diamond shapes (background: 5 squares per centimeter).